# Oxygen microcapsules improve immune checkpoint blockade by ameliorating hypoxia condition in pancreatic ductal adenocarcinoma

Jiangchao Wu [a,b,c,1], Xun Wang [a,b,c,1], Li Chen [d,e,1], Jianing Wang [a,b,c,1], Junlei Zhang [a,b,c], Jianghui Tang [a,b,c], Yongtao Ji [a,b,c], Jinyuan Song [a,b,c], Lin Wang [a,b,c], Yaxing Zhao [a,b,c], Hui Zhang [a,b,c], Taohong Li [a,b,c], Jianpeng Sheng [a,b,c,*], Dong Chen [d,e,**], Qi Zhang [a,b,c,***], Tingbo Liang [a,b,c,****]

[a] Department of Hepatobiliary and Pancreatic Surgery, The First Affiliated Hospital, Zhejiang University School of Medicine, Hangzhou, 310003, China
[b] Zhejiang Provincial Key Laboratory of Pancreatic Disease, The First Affiliated Hospital, Zhejiang University School of Medicine, Hangzhou, 310003, China
[c] Zhejiang University Cancer Center, Zhejiang University, Hangzhou, 310003, China
[d] Department of Medical Oncology, The First Affiliated Hospital, School of Medicine, Zhejiang University, #79 Qingchun Road, Hangzhou, Zhejiang Province, 310003, China
[e] College of Energy Engineering and State Key Laboratory of Fluid Power and Mechatronic Systems, Zhejiang University, Hangzhou, 310027, China

## ARTICLE INFO

## ABSTRACT

*Rationale:* Hypoxia in tumor microenvironment (TME) represents an obstacle to the efficacy of immunotherapy for pancreatic ductal adenocarcinoma (PDAC) through several aspects such as increasing the expression of immune checkpoints or promoting fibrosis. Reversing hypoxic TME is a potential strategy to improve the validity of immune checkpoint blockade (ICB).
*Methods:* Here, we synthesized polydopamine-nanoparticle-stabilized oxygen microcapsules with excellent stabilization, bioavailability, and biocompatibility for direct oxygen delivery into tumor sites by interfacial polymerization.
*Results:* We observed oxygen microcapsules enhanced the oxygen concentration in the hypoxia environment and maintained the oxygen concentration for a long period both *in vitro* and *in vivo*. We found that oxygen microcapsules could significantly improve the efficiency of ICB against PDAC *in vivo*. Mechanismly, combined treatments using oxygen microcapsules and ICB could reduce the infiltration of tumor-associated macrophages (TAMs) and polarized pro-tumor M2 macrophages into anti-tumor M1 macrophages. In addition, combined treatments could elevate the proportion of T helper subtype 1 cells (Th1 cells) and cytotoxic T lymphocytes cells (CTLs) to mediate anti-tumor immune response in TME.
*Conclusion:* In summary, this pre-clinical study indicated that reversing hypoxia in TME by using oxygen microcapsules was an effective strategy to improve the performances of ICB on PDAC, which holds great potential for treating PDAC in the future.

## 1. Introduction

Pancreatic ductal adenocarcinoma (PDAC) is the seventh leading cause of cancer death worldwide, which causes 496,000 new cases and 466,000 deaths per year [1]. Due to its delayed diagnosis and insufficient response to various treatments, PDAC has the most dismal 5-year

---

relative survival rates with approximately 10% [2]. In recent years, targeting immune checkpoints including programmed cell death protein-1 (PD-1) and programmed cell death ligand-1 (PD-L1) has become a potential treatment strategy for various cancers [3]. Nevertheless, PDAC is notorious for its low clinical response to immune checkpoint blockade (ICB) such as anti-PD-1 antibody and anti-PD-L1 antibody [4–6]. Recently, various studies have discovered that the resistance to ICB is in part mediated due to the hypoxic tumor microenvironment (TME) of PDAC featured by the dense physical barrier and insufficient vascularization [7–9]. In addition, hypoxia inducible factor (HIF) is upregulated in PDAC TME, which can increase the expression of PD-L1 and decrease the expression of MHC I [10], thereby dampening the anti-tumor effects of ICB [11,12]. Hence, alleviating the hypoxic condition in TME is a potential treatment strategy to improve the efficacy of ICB for PDAC.

Increasing the partial pressure of oxygen by intravenous oxygen supply is an efficient strategy to reverse the hypoxic conditions in TME [13]. However, intravenous delivery of oxygen might simultaneously cause the potential risk of systemic reactive oxygen species (ROS) exposure. Furthermore, it is infeasible to deliver oxygen directly into the tumor through blood because of its low solubility. Therefore, nanotechnology-based oxygen delivery directly into the tumor sites is a potential tactic to reverse the hypoxic conditions in TME [14,15].

After years of exploration, nanoparticles were regarded as a new modality for cancer therapy [16,17]. Charactered by their small size, abundant surface area, excellent bioavailability, and biocompatibility,
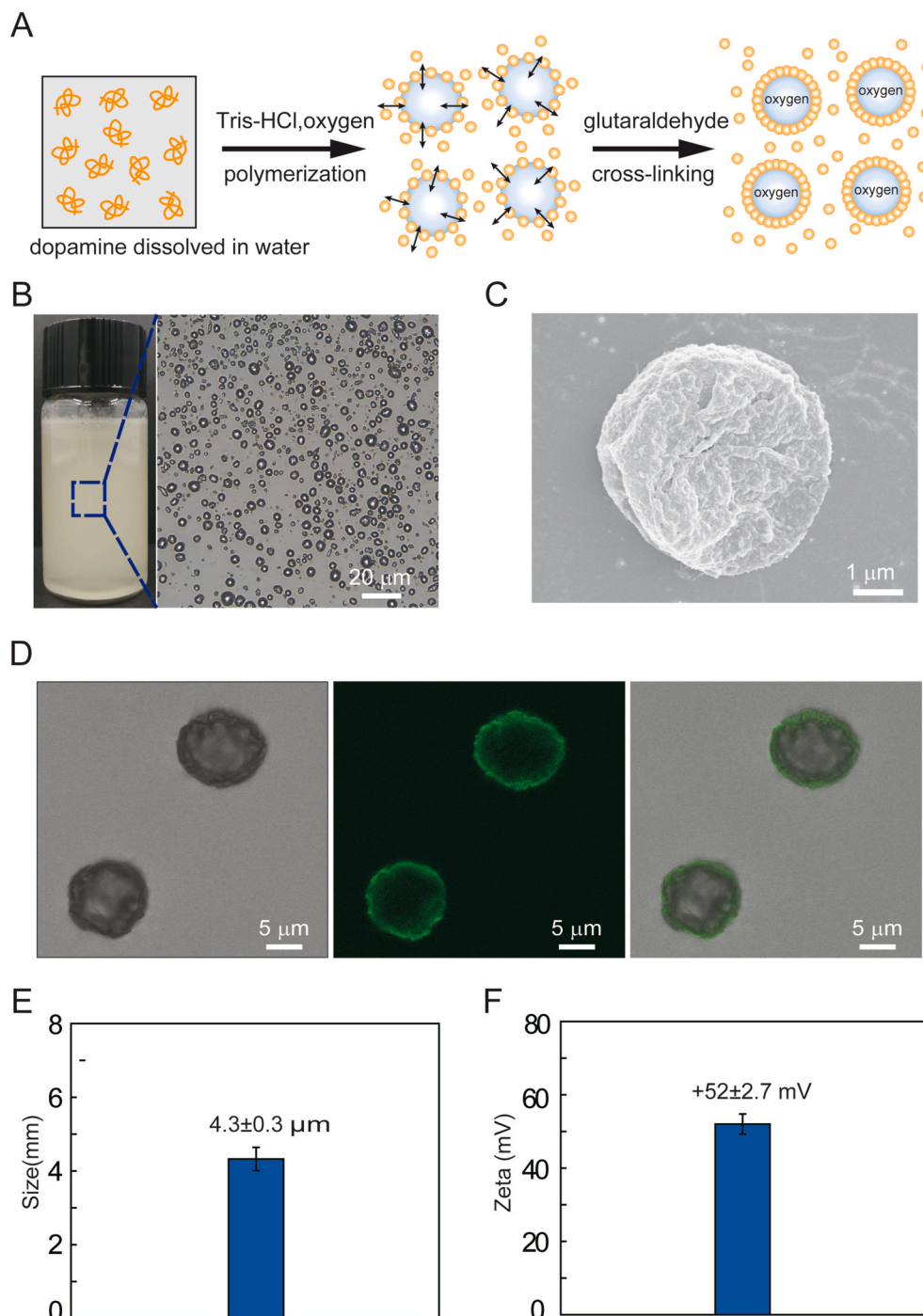


**Fig. 1.** Preparation and characterization of polydopamine-particle-stabilized oxygen microcapsules.

(A). A schematic diagram of the polymerization and cross-linking of polydopamine nanoparticles at the oxygen/water interface to form stable oxygen microcapsules.(B). The representative optical image of oxygen microcapsules stabilized by polydopamine particles. The scale bar was 20 μm (C). The representative SEM image of collapsed oxygen microcapsules stabilized by polydopamine particles. The scale bar was 1 μm. (D). Optical, fluorescent, and overlay images of polydopamine-nanoparticle-stabilized oxygen microcapsule. Polydopamine nanoparticles have fluorescent properties. The scale bars were 5 μm. (E). Size distribution of oxygen microcapsules stabilized by polydopamine particles. Data were presented as the mean ± SD.(F). Zeta potential of oxygen microcapsules stabilized by polydopamine particles. Data were presented as the mean ± SD.

nanoparticles hold great potential to deliver external oxygen into the hypoxic TME safely and effectively [18,19]. However, due to coalescence and oswald ripening, dispersions of oxygen microbubbles are unstable [20–22]. Therefore, it is crucial to develop stable and biocompatible oxygen-loaded delivery systems to reverse the hypoxic conditions in the TME.

In this study, we successfully developed oxygen microcapsules through interfacial polymerization, which encapsulate oxygen in the core of the polydopamine shell. We observed that oxygen microcapsules could significantly improve the efficacy of anti-PD-1 antibody against PDAC *in vivo*. Mechanismly, combined treatments using oxygen microcapsules and anti-PD-1 antibody could alleviate the infiltration of tumor-associated macrophages (TAMs) and polarize pro-tumor M2 macrophages into anti-tumor M1 macrophages. In addition, combined treatments could elevate the proportion of T helper subtype 1 cells (Th1 cells) and cytotoxic T lymphocytes cells (CTLs) to mediate anti-tumor immune response in TME. These results demonstrated that reversing hypoxia in TME by oxygen microcapsules could be a beneficial therapeutic strategy to improve the performances of ICB on PDAC, which holds great potential for treating PDAC in the future.

## 2. Results

### 2.1. Preparation and characterization of polydopamine-particle-stabilized oxygen microcapsules

To prepare nanoparticle-stabilized oxygen microcapsules, polylysine, dopamine, and chitosan were dissolved in water. Then, oxygen was sheared into microbubbles, and dopamine was oxidized at the oxygen/water interface in an alkaline environment to form stable polydopamine nanoparticles [18]. With the help of amino-rich polylysine and chitosan, polydopamine was accelerated to form, which resulted in more uniform polydopamine nanoparticles. The uniform polydopamine nanoparticles could prevent the peroxidation of polydopamine nanoparticles. Finally, polydopamine nanoparticles enriched at the oxygen/water interface temporarily were stabilized by cross-linked via glutaraldehyde (Fig. 1A). As shown in Fig. 1B, oxygen microcapsules were dispersed and stored in water. In addition, we observed strong contrast at the edges of oxygen microcapsules under an optical microscope, due to the difference of refractive index between oxygen and water, suggesting the successful storage of oxygen in the microcapsules (Fig. 1B). Since the tumor microenvironment is widely accepted to be acidic, the stability of the oxygen microcapsule in an acidic environment was also determined by adding 0.5 ml oxygen microcapsule in 5 ml
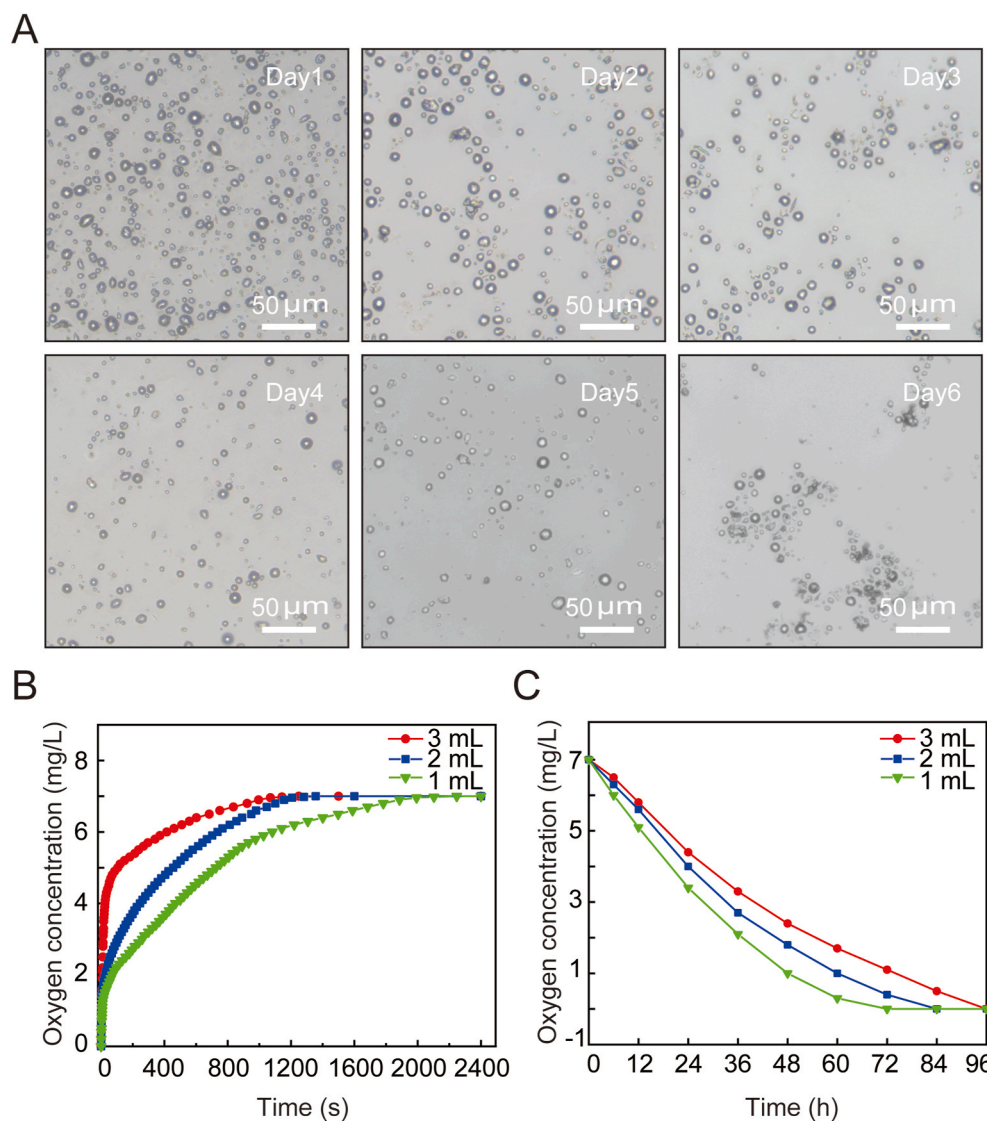


**Fig. 2.** Oxygen transport performance of polydopamine-particle-stabilized oxygen microcapsules (A). Optical image of the stable oxygen microcapsule overtime. Oxygen microcapsules shrunk and collapsed after the release of oxygen. The scale bars were 50 μm. (B). The oxygen concentration was monitored over time after the addition of 1 ml, 2 ml, and 3 ml of oxygen microcapsule dispersion into 10 ml deoxygenated PBS buffer, respectively.(C). The oxygen concentration in the dispersion was monitored when the oxygen-saturated dispersion was placed in a nitrogen environment.

HCl-containing water of pH = 5.2, and the result was presented in Fig. S1A.

To examine the surface morphology of oxygen microcapsules, scanning electron microscopy (SEM) was used. We observed a rough solid shell of the oxygen microcapsules (Fig. 1C). The SEM image of

uncracked and cracked oxygen microcapsules were shown in Fig. S1B. Fluorescent confocal microscope images revealed the thin shell formed by polydopamine and the oxygen core (Figure.1D, Fig. S1C). Oxygen microcapsules stabilized by polydopamine nanoparticles could disperse well in water and the size of oxygen microcapsules ranged from 3 µm to
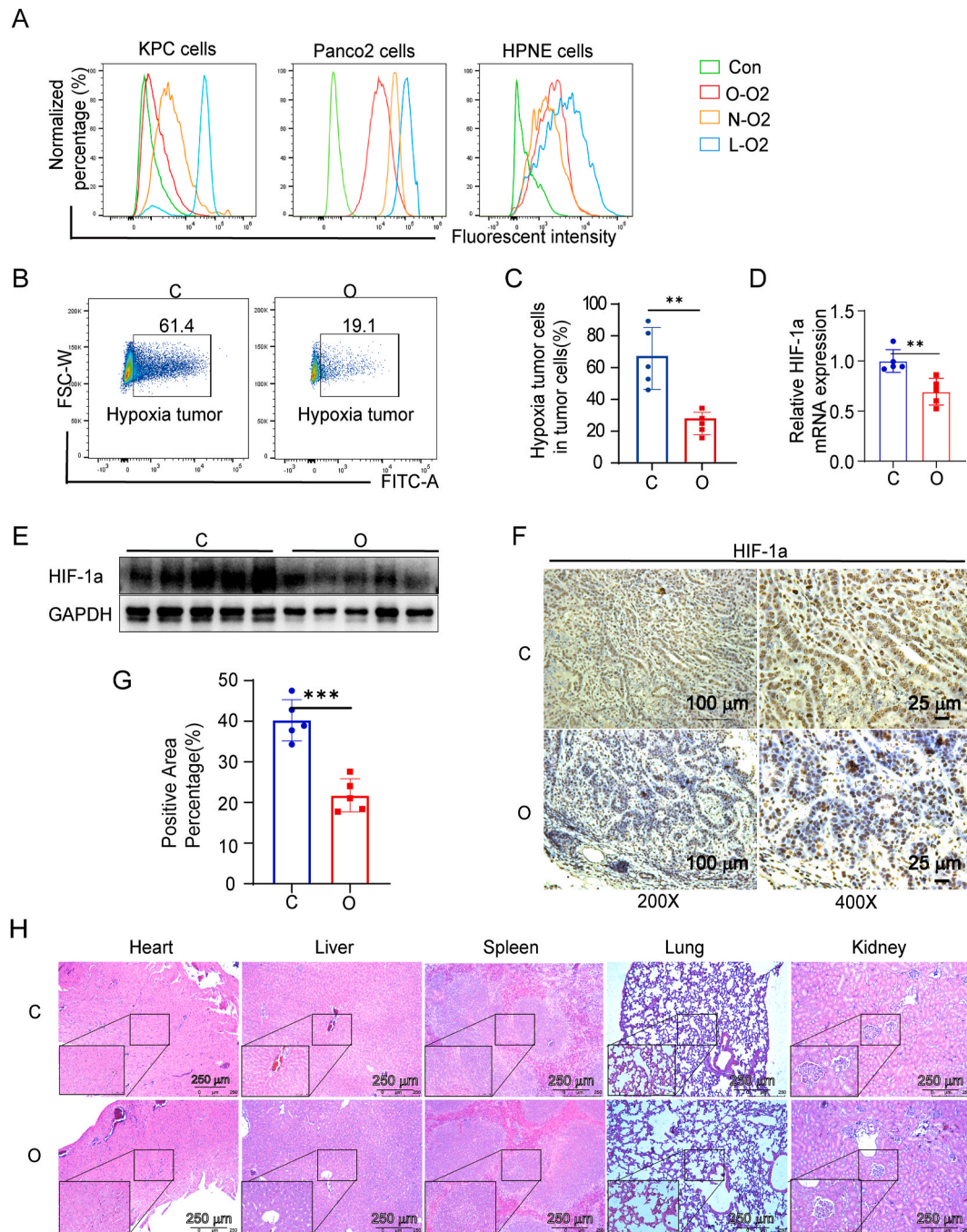


**Fig. 3.** Oxygen microcapsules reversed the hypoxia condition *in vitro* and *in vivo*
(A). The distribution fluorescent intensity of KPC, Panc02 pancreatic cancer cell lines, and normal pancreas cell HPNE cultured from Con group, N–O2 group, L-O2 group, and O–O2 group. Con group: cells cultured in normoxic conditions without incubation with the hypoxia probe; N–O2 group: cells were cultured in normoxic conditions; L-O2 group: cells were treated with a low oxygen level (1% O2) in a hypoxic chamber; O–O2 group: cells were maintained in a hypoxic environment (1% O2) for 18 h followed with treatment with oxygen microcapsules. (B). The representative FACS plots of hypoxia in EpCAM + tumor cells from tumor-bearing mice in the C group and the O group.(C). The mean fluorescent intensity of EpCAM + tumor cells from tumor-bearing mice in the C group and the O group. **p < 0.01. (D). mRNA expression levels of HIF-1α in tumor samples obtained from orthotopic PDAC tumor model in C group and O group were quantified by quantitative qRT-PCR. (E). Protein expression levels of HIF-1α in tumor samples obtained from orthotopic PDAC tumor model in C group and O group were assessed by Western blot. (F–G). The representative images and further quantification of HIF-1α in tumor samples were obtained from the orthotopic PDAC tumor model in the C group and the O group. Scale bars: 200 × : 100 µm; 400 × : 25 µm. (H). Safety evaluation of mice from different groups. H&E staining micrographs of heart, liver, spleen, kidney, and lung from each group with various treatments. Scale bars: 100 × : 250 µm; 400 × : 50 µm.

6.5 μm with an average size of 4.3 ± 0.3 μm and the zeta potential ranged from 37 to 68 mV with an average Zeta potential of 52 ± 2.7 mV (Fig. 1E, F, Figs. S2A and B), which resulted from the adsorption of positively-charged polylysine and chitosan on the surface.

Due to the higher oxygen concentration in the oxygen microcapsules, oxygen will gradually diffuse out and keep stable without obvious change for at least 7 days (Fig. 2A). Next, we tested the oxygen transport capacity of oxygen microcapsules. We first examined the oxygen delivery performance of polydopamine nanoparticles in an anoxic environment with purging nitrogen. The oxygen microcapsules were added to deoxygenated PBS buffer to monitor the change of oxygen concentration over time. We found oxygen could rapidly diffuse into the hypoxic PBS buffer driven by the oxygen concentration gradient, resulting in increased oxygen concentration in the medium. For example, the oxygen concentrations with 1 mL, 2 mL, or 3 mL dispersions of oxygen microcapsules reached 7 mg/L at approximately 33 min, 23 min, and 20 min, respectively (Fig. 2B). In addition, oxygen-saturated PBS solutions with oxygen microcapsule dispersions were placed in a nitrogen environment to monitor the sustained release of oxygen microcapsules. As shown in Fig. 2C, the oxygen concentrations in the medium with 1 mL, 2 mL, and 3 mL dispersions of oxygen microcapsules in 1 mL oxygen-saturated PBS solutions decreased to 0 mg/L at approximately 72 h, 84 h, and 96 h, respectively. Overall, the above results suggested that polydopamine-nanoparticle-stabilized oxygen microcapsule could be used as an excellent oxygen delivery vehicle.

## 2.2. Oxygen microcapsules alleviated the hypoxic condition in vitro and in vivo

To evaluate the efficiency of oxygen microcapsules in alleviating the hypoxic condition, we assessed the hypoxic condition both *in vitro* and *in vivo*.

The degree of hypoxia of KPC, Panc02 pancreatic cancer cell lines, and normal pancreas cell HPNE with different treatments were examined with a hypoxia probe based on the fluorescent intensity. Fluorescent intensity is positively correlated with the degree of hypoxia. KPC cells were divided into four groups: cells cultured in normoxic conditions without incubation with the hypoxia probe as Con group, cells cultured in normoxic conditions as N–O2 group, cells cultured in a hypoxic condition as L-O2 group, and cells treated with oxygen microcapsules in a hypoxic condition as O–O2 group. The gating strategies of FACS were shown in the scheme described in Fig. S6A. As shown in Fig. 3 A, cells in the L-$O_2$ group had a higher degree of hypoxia than cells in the N–$O_2$ group indicated by the stronger fluorescent intensity. In addition, compared with cells in the L-$O_2$ group, and N–$O_2$ group, cells in hypoxic condition treated with oxygen microcapsules (O–$O_2$ group) showed the least fluorescent intensity reflecting the successful oxygen delivery *in vitro*. Then we performed *In vitro* cytotoxicity analysis to explore what consequence does oxygen microcapsules on the vitality or proliferation of tumor cells. Cytotoxicity of oxygen microcapsules against KPC and Panco2 cells was tested by using cell count kit-8 after treatment with various concentrations of oxygen microcapsules for 24h and 48h. As shown in Fig. S3 A, treatment with oxygen microcapsule resulted in reduced viability and proliferation of KPC and Panco2 cells.

Next, we assessed the effects of oxygen microcapsules on the degree of hypoxia KPC cell line subcutaneous allograft *in vivo* model. Mice were randomly divided into two groups: mice received the vehicle as C group, mice treated with oxygen microcapsules as O group. FACs results demonstrated that oxygen microcapsules could significantly reduce the percentage of hypoxic EpCAM + tumor cells obtained from tumor-bearing mice (Fig. 3B, C, Fig. S6B).

Then we further detect the effects of oxygen microcapsules on the degree of the hypoxia in orthotopic PDAC tumor model which could recapitulate the TME. Hypoxia-inducible factor-1α (HIF-1α) is a canonical marker to reflect the hypoxic condition in TME [23]. Firstly, we analyzed the expression of HIF-1α by q-PCR and Western Blot. The

results demonstrated that oxygen microcapsules could significantly reduce the expression of HIF-1α on a transcriptional and protein level obtained from orthotopic PDAC tumor samples (Fig. 3D and E). Immunohistochemistry was performed to detect HIF-1α changes in different groups. Our results showed an obvious reduction of HIF-1α by the treatment of oxygen microcapsules in the O group compared with the C group (Fig. 3F and G).

Furthermore, we explored the biosafety of oxygen microcapsules *in vivo* to assure further translation application. The biocompatibility of oxygen microcapsules was evaluated by histopathological analysis and biochemical examination. As shown in Figure.3H and Fig. S3B, administration of oxygen microcapsule resulted in no damage to major organs including heart, liver, spleen, kidney, and lung of mice. These results revealed that oxygen microcapsules could efficiently reverse the hypoxic condition both *in vitro* and *in vivo* without any damage to major organs.

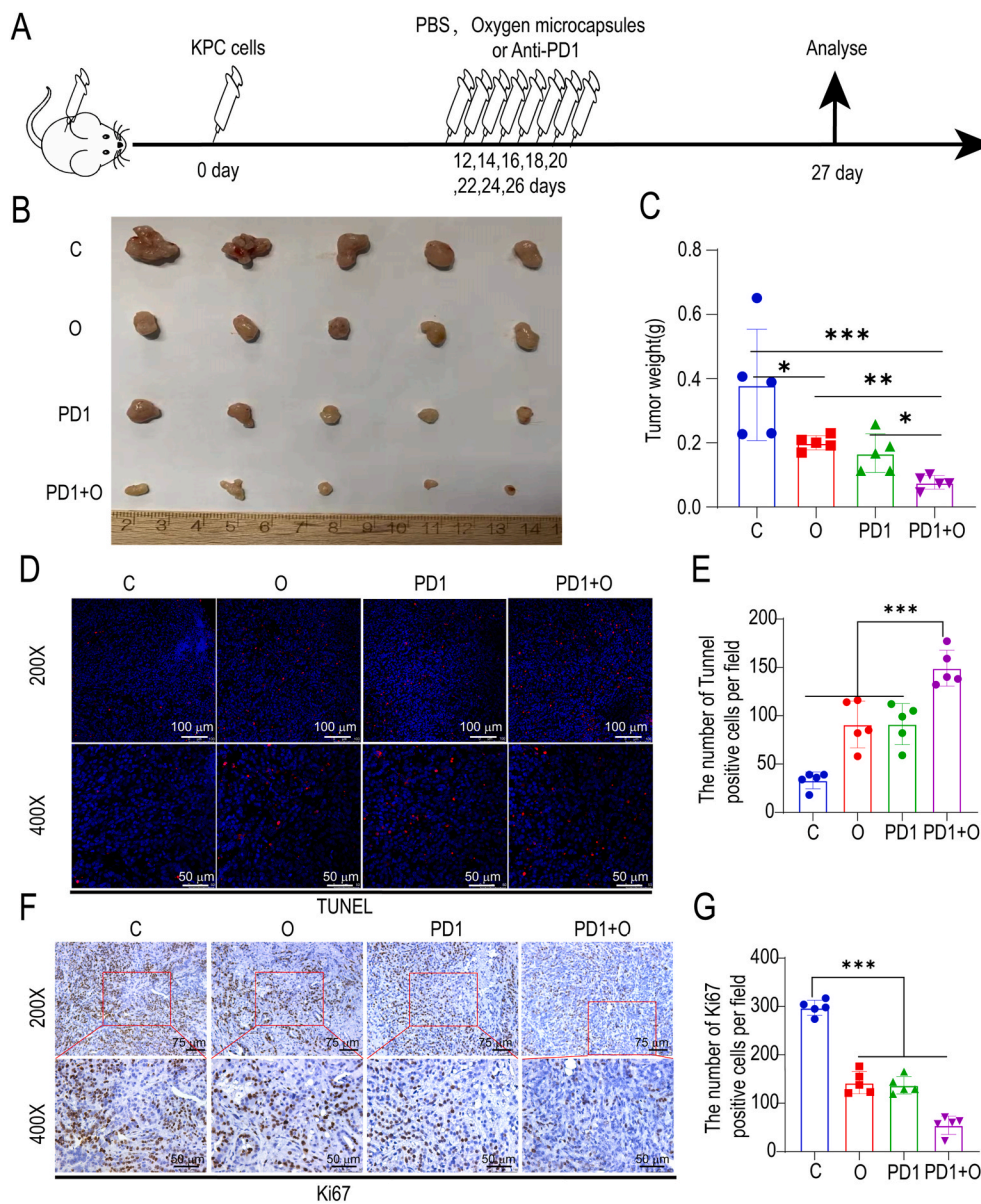## 2.3. Enhanced efficacy of ICB by oxygen microcapsules

Next, in order to explore the effect of oxygen microcapsules on the efficacy of ICB therapy, we treated oxygen microcapsules with or without anti-PD-1 antibody administration in both orthotopic and subcutaneous allograft *in vivo* model for PDAC: mice received the vehicle as C group, mice treated with anti-PD-1 antibody as PD1 group, mice treated with oxygen microcapsules as O group, then mice treated with anti-PD-1 antibody and oxygen microcapsules simultaneously as PD1+O group (Fig. 4A, Figure.S5 A).

Firstly, we established orthotopic PDAC tumor model which is a better *in vivo* model to recapitulate the TME. 10 days after implantation, tumor-bearing mice received an intra-tumoral injection of 100 μL oxygen microcapsules every two days by ultrasound-guided percutaneous injection for a total of 8 times and anti-PD-1 antibody was given by intraperitoneal injection every two days as shown in Fig. 4A. Successful ultrasound-guided percutaneous injection into the intra-tumoral site was verified by the liquid cavity formed after injection (Figs. S4A and B). We found oxygen microcapsule or anti-PD-1 antibody could decrease tumor size compared with the C group. More importantly, a further decrease of tumor size was observed by combination treatment of oxygen microcapsule and anti-PD-1 antibody compared with other treatments (Fig. 4B). The efficacy of different treatments was also evaluated by the tumor weight, which showed that combination treatment of oxygen microcapsule and anti-PD-1 antibody reached better efficacy than other treatments (Fig. 4C), consisting with the results of tumor size. We also explored the effect of oxygen microcapsules on the efficacy of ICB therapy in subcutaneous allograft *in vivo* models. The results were consistent with results in orthotopic PDAC tumor model proved by the tumor volume, tumor size, and the tumor weight (Figs. S5B, D, E). Importantly, we observed no significant loss of mice's weight in these groups, suggesting that mice were tolerated with the combined treatments (Fig. S5C).

In addition, TUNEL assay (indicator for apoptosis) and Ki67 staining (indicator for proliferation) suggested that oxygen microcapsules could promote apoptosis (Fig. 4D and E) and reduce the proliferation (Fig. 4F and G) simultaneously in TME, which could further prove the combination treatment effects of oxygen microcapsule and anti-PD-1 antibody. These *in vivo* results illustrated that oxygen microcapsules could significantly enhance the efficacy of ICB.

## 2.4. Oxygen microcapsules combined with anti-PD-1 antibody promoted immune activation in PDAC

Due to the effects of oxygen microcapsules on reversing the hypoxic condition in TME, we wanted to illustrate the mechanism by which oxygen microcapsules enhanced the efficacy of anti-PD-1 antibody. The changes in immune status of *in vivo* orthotopic PDAC model were assessed after various treatments. Firstly, we analyzed the changes of total immune cells and TAMs. Since the immune-suppressed TME

**Fig. 4.** Oxygen microcapsules enhanced the efficacy of anti-PD-1 antibody *in vivo*. (A). Therapeutic schedule of the various treatments for the tumor-bearing mice. (B). The morphology of the tumors in each group under different treatments (n = 5). (C). Weight of tumors from each group under various treatments. Data are presented as mean ± SEM (n = 5). (D–E). The representative images and further quantification of TUNEL positive cells in tumor samples obtained from orthotopic PDAC tumor model in each group under different treatments (Scale bars: 200 × : 100 μm; 400 × : 50 μm). (F–G). The representative images and further quantification of Ki67 positive cells in tumor samples were obtained from orthotopic PDAC tumor model in each group under different treatments (Scale bars: 200 × : 75 μm; 400 × : 50 μm).

induced by hypoxia, the accumulation of TAMs plays a crucial role in inhibiting T cell-mediated adaptive anti-tumor immunity [24,25].

The gating strategies of FACS were shown in the scheme described in Fig. 5A. As shown in Fig. 5B, we observed oxygen microcapsules combined with an anti-PD-1 antibody could significantly increase the infiltration of $CD45^+$ immune cells in TME when compared with other treatments. The results in Fig. 5C demonstrated that the percentage of TAMs ($CD11b^+F4/80^+$) in the TME declined in the PD1+ O group. Based on the biological function, TAMs can be divided into two subtypes namely M1 anti-tumor macrophages and M2 pro-tumor macrophages. The imbalance of these two subtypes plays a major role in regulating the progress of the tumors. Hence, the changes of M1 and M2 subtypes were analyzed respectively. As shown in Fig. 5D and E, the proportion of M1 macrophages was significantly increased in the PD1+ O group compared with that in other groups, the lowest proportion of M2 macrophages was observed in the PD1+ O group. In summary, anti-PD-1 antibody combined with oxygen microcapsules could increase the proportion of immune cells in TME. Simultaneously, combined treatments reduced the number of TAMs in the TME and polarized pro-tumor M2 macrophages into anti-tumor M1 macrophages. As we know, myeloid-derived

suppressor cells (MDSCs) are major immunosuppressive cells in TME. To further investigate the influence on the infiltration of MDSCs in the TME, MDSCs in the tumors were detected by flow cytometry after various treatments. According to Fig. S7, we found there was no significant change in the portion of $CD11b^+CD45^+$ cells, G-MDSCs (Dead dye$^-$CD45$^+$CD11b$^+$ Ly6C$^-$Ly6G$^+$), M-MDSCs (Dead dye$^-$CD45$^+$CD11b$^+$ Ly6C$^+$Ly6G$^-$).

Next, we performed FACS to analyze the changes of T cell-mediated adaptive anti-tumor immunity. The gating strategies for the analysis of lymphocytes were shown in Fig. 6A. Firstly, we explored the change of $CD8^+$ T and $CD4^+$ T cells, which are the two major subtypes of T cells. The proportion of $CD8^+$ T cells indicated no difference in different groups (Fig. 6B). However, it was surprising that CTLs (Granzyme B$^+$ $CD8^+$ T Cells) in the PD1 + O group were significantly higher than those in the C groups and O group (Fig. 6C). Additionally, oxygen microcapsules in combination with an anti-PD-1 antibody could reduce the infiltration of $CD4^+$ T cells in TME (Fig. 6D). While, the remaining $CD4^+$ T cells were Th1 cells (IFN-γ$^+$ $CD4^+$ T Cells) (Fig. 6E), which mediated anti-tumor immunity [26,27]. In addition, we found the proportion of Tregs in TME was reduced in the O group and the PD1 + O group
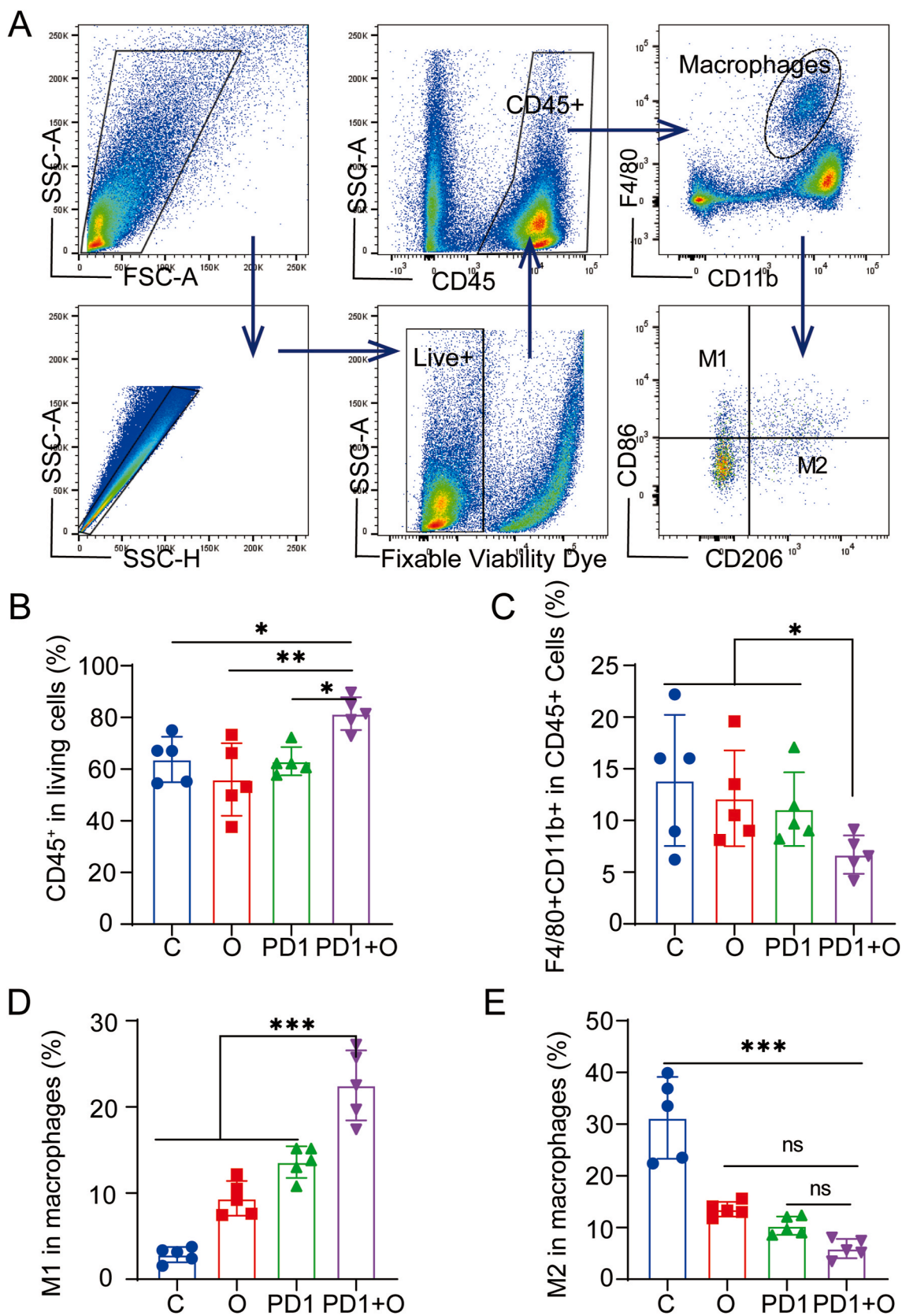
**Fig. 5.** Oxygen Microcapsules combined with anti-PD-1 therapy activated macrophage-mediated adaptive anti-tumor immunity
(A). Gating strategy of FACS analysis for detecting CD45$^+$ cells, TAMs, M1 macrophages, and M2 macrophages in the TME from the tumor-bearing mice with different treatments. (B–E). Statistic results for the proportions of CD45$^+$ cells, TAMs, M1 macrophages, M2 macrophages in the TME of each group. Data were presented as the mean ± SEM (n = 5, per group). *p < 0.05, **p < 0.01, ***p < 0.001.
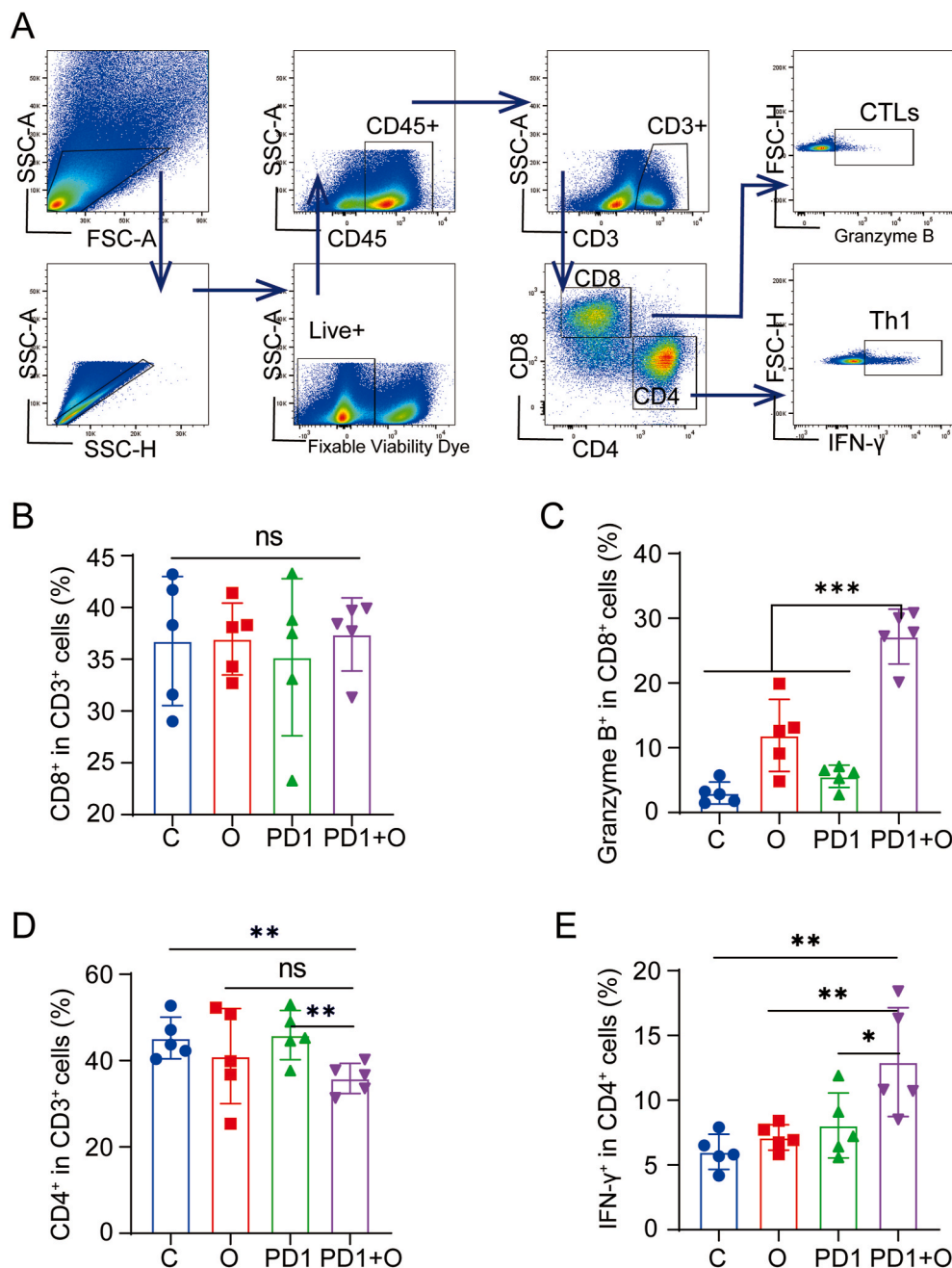
**Fig. 6.** Oxygen Microcapsules combined with anti-PD-1 activated T cell-mediated adaptive anti-tumor immunity (A). Gating strategy of FACS analysis for detecting CTLs (Granzyme B + CD8$^+$ T Cells) and Th1 cells (IFN-γ+ CD4$^+$ T Cells) in the TME from the tumor-bearing mice with different treatments. (B–E). Statistic results for the proportions of CD8$^+$ cells, CD4$^+$ cells, CTLs (Granzyme B + CD8$^+$ T Cells), and Th1 cells (IFN-γ+ CD4$^+$ T Cells) in the TME of each group. Data were presented as the mean ± SEM (n = 5, per group). *p < 0.05, **p < 0.01, ***p < 0.001.

(Figs. S8A and B). The above results suggested that T cell-mediated anti-tumor immunity could be activated by combined treatments using oxygen microcapsules and anti-PD-1 antibody.

Related studies have reported that hypoxia can increase the expression of PD-L1 in the TME to weaken anti-tumor immunity [28]. Therefore, we further analyzed the expression of PD-L1 in TME after various treatments. As shown in Figs. S9A and B, we found that the expression of PD-L1 on tumor cells was downregulated in the O group, PD1 group, and PD1+O group. In summary, these results demonstrated that oxygen microcapsules enhanced the efficacy of anti-PD1 antibody by downregulating the expression of PD-L1 in TME.

## 3. Discussion

Related studies have reported that hypoxic TME can hinder the efficacy of immunotherapy [9]. Thus, reversing the hypoxic tumor microenvironment could be a potential breakthrough point to improve the efficacy of ICB represented by an anti-PD-1 antibody. Two main strategies related to nanotechnology to alleviate hypoxic environment were as follows: (1) Generating oxygen based on nanotechnology in situ by using different approaches like chemical decomposition system [29], water splitting [30], or Catalase (CAT) breaks down $H_2O_2$ [31]. (2) Bringing external oxygen to tumor hypoxia microenvironment like Artificial Red Blood Cells Substitutes (RBCSs) [32,33], PFC-based oxygen carriers (PFOCs) [34]. Nowadays, many of these researches showed successful cancer therapy by alleviating the hypoxic conditions. However, a published essay indicated that less than 1% (median value) of the injected dose of the nanomaterials reached the hypoxic site of the tumor, despite their surface charge composition, size, or composition [35]. This meant that 99% of the injected nanomaterials were most likely accumulated in healthy tissues/organs, which caused negative effects in practical clinical application due to their unassured biocompatibility

and safety. In this pre-clinical study, we successfully synthesized polydopamine-nanoparticle-stabilized oxygen microcapsules, which encapsulated oxygen in the core of the thin shell formed by polydopamine. The original uncross-link polydopamine nanoparticles could only be stable for a short time of several hours. And the cross-linked polydopamine nanoparticles are strongly linked, which improve the stability of oxygen microcapsule to at least a week. The oxygen microcapsules were characterized by excellent stabilization and bioavailability in water. In addition, oxygen microcapsules were excellent and stable oxygen delivery vehicles which could improve the oxygen concentration in a hypoxia environment quickly and sustain the oxygen concentration for a long period time. More importantly, we injected oxygen microcapsules directly into the tumor by ultrasound-guided percutaneous injection (Fig. S4). Ultrasound-guided intra-tumoral injection of medicine is a quite innovative drug delivery technique that have been considered as an efficient method for oncotherapy [36,37]. Ultrasound-guided percutaneous injection of oxygen microcapsules in the internal part of the tumor could assure most of the material remained inside of the tumor. This might ensure biosafety in future clinical applications than other nanomaterials. Besides, ultrasound-guided intra-tumoral injection would cause minimal invasive damage to the patients and allow multiple injections. Thus, intra-tumoral injection of oxygen microcapsules via ultrasound-guided technique holds great potential for future clinical therapy.

Several previous reports have shown that dual inhibition of the PD-1 axis and hypoxia is a potential strategy to enhance the therapeutic efficiency of ICB [38]. Here, we found oxygen microcapsules could significantly improve the efficiency of anti-PD-1 antibody against PDAC *in vivo* accompanied with no damage to major organs. Mechanismly, combined treatments could reduce the infiltration of TAMs and switch the pro-tumor M2 phenotype toward the anti-tumor M1 phenotype. These results were consistent of the findings of previous studies [24,39]. In addition, combined treatments using oxygen microcapsules and anti-PD-1 antibody can elevate the proportion of CTLs and Th1 cells in TME. Furthermore, oxygen microcapsules were able to reduce the expression of PD-L1 on tumor cells. Our results showed that anti-PD-1 therapy work better in a context where PD-L1 is downregulated which was consistent with previous studies [40–42]. We may consider it as "icing on the cake" which means that in the context where PD-L1 is downregulated, the remaining PD-L1 would still bind with PD-1 to suppress immune activity. Under such circumstances, anti-PD-1 antibody suppressed binding of PD-1 and PD-L1 to promote immune activity in the context where PD-L1 is downregulated. The above results validated the feasibility of promoting the anti-PD-1 antibody effects by co-delivery of oxygen microcapsules.

The major limitation of the current study is the oxygen delivery method. Although we solved the intra-tumoral injection via ultrasound-guided injections *in vivo*, such a technique may cause obstacles for future clinical application for oxygen microcapsules. To solve this problem, the polymer shell of microcapsules could be modified with other targeting moieties such as folic acid to target folic acid receptor-positive cancer cells. And other immunostimulatory agents such as toll-like receptor agonists could be filled into the microcapsules to further enhance the anti-tumor response.

In summary, our pre-clinical study indicated that reversing hypoxia in TME by using oxygen microcapsules was an effective strategy to improve the performances of ICB on PDAC, which holds great potential for clinical application in the future.

## 4. Materials and methods

### 4.1. Preparation of oxygen microcapsules

20 mg dopamine (hydrochloride, MW = 189.6 g/mol, Aladdin Biochemical Technology Corporation, China), 120 mg chitosan quaternary ammonium salt (Yuanye Bio-Technology Corporation, China), and

10 mg polylysine (BR, 95%, Nanjing Herbaceous Source Biotechnology Corporation, China) were dissolved in 10 mL deionized water. Then the solution was added with 1 mL Tris salt buffer solution of pH = 8.5 (Tris (hydroxymethyl) aminomethane, 99.5%, J&K Scientific Corporation, China) after 20 min of ultrasonication. Oxygen (Purity 99.99%) was introduced at a flow rate of 1 L/min when the pH of the solution was adjusted to alkaline. The solution was homogenized by a homogenizer (EJ200-SH, Shanghai Specimen and Model Factory, China) for 2.5 min at the rotation speed of 12000 rpm followed by the addition of 1 mL 4% glutaraldehyde solution (AR, 50% in $H_2O$, Aladdin Biochemical Technology Corporation, China). The above solution was then homogenized for an extra 5 min at 12000 rpm and stirred for 30 min at 1000 rpm to form stable oxygen microcapsules. A filter paper with a porosity of 11 μm (Cat No 1001–090, Whatman) was used to remove residual polydopamine nanoparticles and excess solvents. Oxygen microcapsules were washed three times by oxygen-enriched water and stored in oxygen-enriched water.

In addition, the stability of oxygen microcapsule in an acidic environment was also determined by adding 0.5 ml oxygen microcapsule in 5 ml HCl-containing water of pH = 5.2.

### 4.2. Characterization of oxygen microcapsules

A scanning electron microscope (SEM, SU8010, Hitachi) was used to determine the size or morphology of oxygen microcapsules. In order to quantify the size distribution or zeta potential, a Malvern Zetasizer (Nano ZS, Malvern Instruments) was applied.

### 4.3. Measurement of oxygen delivery performances

Pure nitrogen (N2) gas (Purity 99.99%) was used to deoxygenate 1x Phosphate Buffer Saline (PBS) (Cienry Zhejiang, China) at room temperature to mimic a hypoxic environment. 1 mL, 2 mL, and 3 mL dispersions of oxygen microcapsules were added to 5 mL deoxygenated PBS buffer, respectively. The changes in oxygen concentration over time were monitored by a dissolved oxygen analyzer (JPB-607A, Shanghai INESA Scientific Instrument Corporation). The concentration of oxygen microcapsules in water for oxygen delivery performances was about 1 mL oxygen microcapsules in 1 mL water. The increased content of oxygen-derived from oxygen dissolved in water was limited as compared to oxygen microcapsules. Subsequently, samples were placed in the nitrogen environment and the oxygen concentrations were measured every 12 h, respectively.

### 4.4. Cell culture and reagents

The murine PDAC cell line KPC which was derived from the LSLKras$^{G12D/+}$; LSL-Trp53$^{R172H/+}$; Pdx1-Cre spontaneous mouse PDAC model, was a kind of gift from Prof. Raghu Kalluri's laboratory (Department of Cancer Biology, Division of Science, MD Anderson Cancer Center, Houston, TX, USA). KPC cells were cultured in McCoy's 5A medium (Cienry Zhejiang, China) supplemented with 10% fetal bovine serum (FBS, Gibco) and 1% penicillin/streptomycin (Cienry Zhejiang, China). The human normal pancreas cell HPNE and mouse pancreatic cancer cell Panc02 was cultured in DMEM medium (Cienry Zhejiang, China) + 10% FBS and supplemented with 1% penicillin/streptomycin (Cienry Zhejiang, China). Cells were cultured in a humidified cell incubator with 5% $CO_2$ at 37 °C. For the hypoxic culture, cells were cultured in a sealed hypoxia chamber (Thermal Tech, Orlando, FL, USA) with 1% $O_2$. Specifically, cells were exposed to a hypoxic environment (1.0% $O_2$ balanced by $CO_2$ and $N_2$) for the indicated duration until cells reached approximately 60% confluence in normoxic conditions. In order to explore the hypoxia improvement *in vitro,* cells were divided into three groups: Con group, N–$O_2$ group, L-$O_2$ group, and O–$O_2$ group. Con group: cells cultured in normoxic conditions without incubation with the hypoxia probe; N–$O_2$ group: cells were

cultured in normoxic conditions; L-O$_2$ group: cells were treated with a low oxygen level (1% O$_2$) in a hypoxic chamber; O–O$_2$ group: cells were maintained in a hypoxic environment (1% O$_2$) for 18 h followed with treatment with oxygen microcapsules at 18 h and 21 h of culture, respectively. Then cells in the three groups were incubated with the hypoxia green reagent (Cat: H20035; Thermal Tech, Orlando, FL, USA) at 21 h after culture. After 3 h of incubation, cells in the three groups were experienced FACS analysis. All measurements were performed in triplicate.

### 4.5. In vitro cytotoxicity and in vivo biosafety evaluation

The cytotoxicity of oxygen microcapsules *in vitro* was measured using the cell count kit-8 (CCK-8; Dojindo; Kumamoto, Japan). Mouse pancreatic cancer cell KPC and Panc02 cells were seeded into 96-well plates at $5 \times 10^3$ cells/well. The media was removed after 24 h, and replaced with media containing different concentrations of oxygen microcapsules. After 24h or 48h incubation, Cell Counting Kit-8 solution was used to detect the cell viability. Briefly, 100 μL serum-free medium with 10 μL Cell Counting Kit-8 solution inside was added to each well. After 2 h incubation, the cell viability was measured using a Molecule Devices spectrophotometer at 450 nm wavelength.

For biosafety Evaluation *in vivo*, mice major organs including the lungs, liver, spleen, and kidneys were extracted for histological analyses. Serum levels of total protein (TP), Albumin (ALB), Uric acid ( UA ) , Alanine aminotransferase (ALT), creatinine ( GERA ) , total bilirubin (TBIL), and urea (UERA) were evaluated by a liver or renal function activity assay kit (servicebio, China).

### 4.6. Animal model

Twenty male C57BL/6 mice at 6-week-old were purchased from the model animal research center of Nanjing University and bred in an SPF facility of the First Affiliated Hospital, Zhejiang University. To establish an orthotopic PDAC tumor model, $5 \times 10^5$ KPC cells in 25 μl PBS including 10 μl Matrigel were injected into the pancreas using a sterile insulin needle through an incision on the left abdomen. Cohorts of mice were randomly divided into four groups: C group, PD1 group, O group, and PD1+O group. C group 10 days after implantation: mice were treated as the control group; O group: mice were treated with 100 μL dispersion of oxygen microcapsules via intratumoral injection by ultrasound-guided percutaneous injection every two days for two weeks (Figs. S3A and B); PD1 group: mice were treated with 200 μg/dose anti-PD-1 antibody (BE0146, clone RMP1-14, BioXCell) via intraperitoneal injection every two days for two weeks. PD1+O group: mice were simultaneously treated with anti-PD-1 antibody and oxygen microcapsules. The concentration of oxygen microcapsules used for intratumoral injection was about 1 mL oxygen microcapsules in 0.25 mL water. The mice were sacrificed after 2 weeks of treatment and the tumor was weighted. Tumors tissues were collected for further histopathologic analysis and fluorescence-activated cell sorting (FACS) analysis. To establish a subcutaneous allograft *in vivo* model, $5 \times 10^5$ KPC cells in 50 μl PBS were implanted into the right flank of twenty male C57BL/6 mice at 6-week-old. Once the size of the subcutaneous allograft tumor reached about 5 mm × 5 mm, tumor-bearing mice have received the same treatments in the orthotopic PDAC tumor model. Tumor volume was measured every two days and calculated according to the formula: $V = 1/2$ (length × width$^2$). The mice were sacrificed after 2 weeks of treatment and the tumor were weighted. Tumors tissues was collected for further fluorescence-activated cell sorting (FACS) analysis. Animal experiments were approved by the Animal Care and Medical Ethics Committee of the First Affiliated Hospital, Zhejiang University.

### 4.7. Western blotting analysis

For western blotting analysis, total protein from tissues was

extracted using Whole Cell Lysis Assay (KGP250, Keygen biotech, Nanjing, China). Protein concentrations were measured by bicinchoninic acid (BCA) reagent (P0012 Beyotime Biotechnology) using a Molecule Devices spectrophotometer. Equal amounts of protein were resolved in NuPAGE LDS sample buffer (NP0007, Thermo Fisher Scientific) and heated at 100 °C for 5 min. After being separated by SDS–PAGE, the separated protein was transferred onto polyvinylidene difluoride (PVDF) membranes (Millipore) which were blocked with 5% non-fat milk and incubated at 4 °C for overnight with the primary antibodies including GAPDH (ab181602, Abcam) and HIF-1α (PA1-16601, Thermo Fisher Scientific), followed by the corresponding secondary antibodies. Then the blots were detected using a ChemiScope- Touch (Clinx Science Instruments).

### 4.8. Real-time RT-PCR analyses

Total RNAs from tissues were extracted using RNAfast200 total RNA isolation kit (220011, Fastagen, China). After measuring the concentration of tissue RNA by Thermo Scientific™ NanoDrop™, total RNA was reverse transcribed into cDNA using a PrimeScript RT reagent kit (RR047A, Takara) according to the manufacturer's instructions. Then qRT-PCR was conducted by using TB Green Premix Ex Taq™ II (RR820A, Takara) in a real-time PCR machine (Applied Biosystems 7500 Fast Real-Time PCR System, Applied Biosystems). The relative expression of genes was calculated by 2– (ΔCtexperimental group–ΔCtcontrol group). The primer sequences were as follows:

Mouse GAPDH:
Forward 5′-CCTCGTCCCGTAGACAAAATG-3′;
Reverse 5′-TTGACTGTGCCGTTGAATTTG-3′.
Mouse HIF-1α:
Forward 5′-GAGGTGGATATGTCTGGGTTG-3′;
Reverse 5′-AGGGAGAAAATCAAGTCGTGC-3′.

### 4.9. Hematoxylin-eosin staining, immunohistochemical and immunofluorescence staining

Immunohistochemical were performed to analyze the Ki67, HIF-1α, and hematoxylin-eosin staining (H&E) as previously described [43]. Briefly, formalin-fixed, paraffin-embedded tumor tissue samples were cut into 4-μm thick sections. Sections were processed for H&E. For immunohistochemistry staining, sections were deparaffinized in xylene and rehydrated in ethanol followed with antigen retrieval at 100 °C in 10 mM sodium citrate buffer for 10 min. Then, 3% H$_2$O$_2$ was used to quench endogenous peroxidase. After blocking with 3% BSA, sections were incubated with anti–HIF–1α (ab114977, Abcam, 1:200), anti-Ki67 (ab16667, Abcam, 1:200) antibodies overnight at 4 °C, respectively. The slides were then incubated with HRP-conjugated secondary antibodies (A0208, A0216, Beyotime Institute of Biotechnology, Shanghai, China) at room temperature for 50 min. The slides were observed under a microscope (Leica, Heidelberg, Germany) after being counterstained with hematoxylin and developing with DAB (ZLI-9019, ZSGB-BIO, Beijing, China). The various organs provided for assessment of damage from these oxygen microcapsules came from the same cohort of mice receiving tumor cells. In addition, all mice in each cohort were assessed and representative pictures of the whole group were displayed in the manuscript. For immunofluorescence staining, a terminal deoxynucleotidyl transferase (TdT)-mediated dUTP-biotin nick end labeling (TUNEL) assay was performed using the one-step TUNEL kit (C1089, Beyotime Institute of Biotechnology, Shanghai, China) according to the instructions. The slides were observed by cofocal (Leica, Heidelberg, Germany). The images were analyzed by using ImageJ 1.53c software (National Institutes of Health, Bethesda, USA).

### 4.10. FACS analysis

Single-cell suspensions from tumor-bearing mice were prepared by

mechanical and enzymatic digestion in culture medium containing 0.6 mg/mL collagenase IV (17104019, Gibco),0.01 mg/mL DNase I (11284932001, Merck) and 2% FBS at 37 °C for 1 h. Single-cell suspensions were resuspended in 36% Percoll (P4937, Sigma) and centrifuged at 300 g for 5 min followed with red blood cell lysis by using blood lysis buffer (555899, BD) for 10 min at RT. After red blood cell lysis, the cell suspensions were blocked with FC Block (156604, BioLegend) on ice for 10 min. Then Single-cell suspensions were stained with the following antibodies. Antibodies including CD45-BV605 (Clone:30-F11; 563053; 1:600; BD Biosciences), CD45-BV785 (103149; Clone:30-F11; 1:600; BioLegend), CD3-FITC (Clone:17A2; 100203; 1:600; BioLegend), CD4-PerCP-Cy™5.5 (Clone:RM4-5; 561115; 1:600, BD Biosciences), CD8-BV510 (Clone:53–6.7; 563068; 1:600; BD Biosciences), CD25-AF700 (Clone:PC61; 102024; 1:600; BioLegend), Fxop3-APC (Clone:FJK-16s; 17-5773-82; 1:600; Thermofisher), IFN-γ-PE-cy7 (Clone:XMG1.2; 505826; 1:600; BioLegend), Granzyme B-BV421 (Clone:QA18A28; 396414; 1:600; BioLegend), F4/80-PE (Clone:T45-2342; 565410; 1:600; BD Biosciences), CD11b-Buv395 (Clone:OX-42; 743983; 1:600; BD Biosciences), CD86-PE-cy7 (Clone:GL1; 560582; 1:600; BD Biosciences), CD206-APC (Clone: C068C2; 141708; 1:600; BioLegend), Ly6C-Bv605 (Clone:AL-21; 563011; 1:600; BD Biosciences), Ly6G-FITC (Clone:1A8; 551460; 1:600; BD Biosciences), PD-L1-BV650 (Clone:MIH5; 740614; 1:600; BD Biosciences), and EpCAM-BV510 (Clone:G8.8; 747748; 1:600; BD Biosciences). Flow cytometry analysis was performed on a BD Fortessa 5 laser flow cytometer (BD Bioscience, Fortessa).

### 4.11. Detection of oxygen levels

To detect the levels of oxygen in live cells, hypoxia green reagent (Thermo Fisher, Cat: H20035) was used according to the manufacturer's instructions: 1 mL of $1 \times 10^6$ cells was incubated with 1 μm of 1 mM hypoxia green reagent for 3 h followed with FACS analysis by detecting the fluorescent intensity, which is proportional to the number of hypoxic cells labeled by hypoxia green reagent.

### 4.12. Statistical analysis

Data are presented as the mean ± SD or SEM. GraphPad Prism 6 and FlowJo.10 were used for statistical analysis. In order to analyze the statistically significant differences between the two groups, we employed unpaired Student's t-tests. One-way analysis of variance with the Bonferroni post-test was used to identify significant differences for three or more groups. Significant differences between the groups are indicated by a *P*-value less than 0.05.

### Declaration of interests

The authors declare no competing interests.

### Data availability statement

The data that support the findings of this article will be shared at reasonable request to the corresponding author.

### CRediT authorship contribution statement

**Jiangchao Wu:** Methodology, Flow cytometry panel, Formal analysis, Writing – original draft. **Xun Wang:** Methodology, Flow cytometry panel, Formal analysis, Writing – original draft, Funding acquisition. **Li Chen:** Methodology, Formal analysis, Pathological support. **Jianing Wang:** Methodology, Writing – original draft. **Junlei Zhang:** Pathological support. **Jianhui Tang:** Pathological support. **Yongtao Ji:** Pathological support. **Jinyuan Song:** Pathological support. **Lin Wang:** Investigation. **Yaxing Zhao:** Investigation. **Hui Zhang:** Investigation. **Taohong Li:** Investigation. **Jianpeng Sheng:** Conceptualization, Flow cytometry panel, Supervision, Formal analysis, Writing – original draft, Writing – review & editing, Funding acquisition. **Dong Chen:** Conceptualization, Supervision, Writing – review & editing. **Qi Zhang:** Conceptualization, Supervision, Funding acquisition. **Tingbo Liang:** Conceptualization, Supervision, Writing – review & editing, Funding acquisition.

### Abbreviations

| | |
|---|---|
| TME | tumor microenvironment |
| PDAC | pancreatic ductal adenocarcinoma |
| ICB | immune checkpoint blockade |
| TAMs | tumor-associated macrophages |
| PD-1 | programmed cell death protein-1 |
| PD-L1 | programmed cell death ligand-1 |
| HIF | hypoxia-inducible factor |
| ROS | reactive oxygen species |

### Appendix A. Supplementary data

Supplementary data to this article can be found online at https://doi.org/10.1016/j.bioactmat.2022.05.022.

### References

[1] H. Sung, J. Ferlay, R.L. Siegel, M. Laversanne, I. Soerjomataram, A. Jemal, et al., Global cancer statistics 2020: GLOBOCAN estimates of incidence and mortality worldwide for 36 cancers in 185 countries, CA Cancer J Clin 71 (2021) 209–249.

[2] R.L. Siegel, K.D. Miller, H.E. Fuchs, A. Jemal, Cancer statistics, 2021, CA Cancer J Clin 71 (2021) 7–33.

[3] X. Xia, R. Li, P. Zhou, Z. Xing, C. Lu, Z. Long, et al., Decreased NSG3 enhances PD-L1 expression by Erk1/2 pathway to promote pancreatic cancer progress, Am. J. Cancer Res. 11 (2021) 916–929.

[4] H. Ying, P. Dey, W. Yao, A.C. Kimmelman, G.F. Draetta, A. Maitra, et al., Genetics and biology of pancreatic ductal adenocarcinoma, Genes Dev. 30 (2016) 355–385.

[5] R.A. Skelton, A. Javed, L. Zheng, J. He, Overcoming the resistance of pancreatic cancer to immune checkpoint inhibitors, J. Surg. Oncol. 116 (2017) 55–62.

[6] A. Henriksen, A. Dyhl-Polk, I. Chen, D. Nielsen, Checkpoint inhibitors in pancreatic cancer, Cancer Treat Rev. 78 (2019) 17–30.

[7] C. Feig, A. Gopinathan, A. Neesse, D.S. Chan, N. Cook, D.A. Tuveson, The pancreas cancer microenvironment, Clin. Cancer Res. 18 (2012) 4266–4276.

[8] D.P. Zandberg, A.V. Menk, M. Velez, D. Normolle, K. DePeaux, A. Liu, et al., Tumor hypoxia is associated with resistance to PD-1 blockade in squamous cell carcinoma of the head and neck, J. Immunother. Cancer 9 (2021).

[9] M. Jiang, B. Qin, L. Luo, X. Li, Y. Shi, J. Zhang, et al., A clinically acceptable strategy for sensitizing anti-PD-1 treatment by hypoxia relief, J. Contr. Release 335 (2021) 408–419.

[10] S. Chouaib, M.Z. Noman, K. Kosmatopoulos, M.A. Curran, Hypoxic stress: obstacles and opportunities for innovative immunotherapy of cancer, Oncogene 36 (2017) 439–445.

[11] A. Palazon, P.A. Tyrakis, D. Macias, P. Velica, H. Rundqvist, S. Fitzpatrick, et al., An HIF-1alpha/VEGF-A Axis in cytotoxic T cells regulates tumor progression, Cancer Cell 32 (2017) 669–683 e5.

[12] M.Z. Noman, S. Buart, P. Romero, S. Ketari, B. Janji, B. Mari, et al., Hypoxia-inducible miR-210 regulates the susceptibility of tumor cells to lysis by cytotoxic T cells, Cancer Res. 72 (2012) 4629–4641.

[13] M.S. Khan, J. Hwang, K. Lee, Y. Choi, K. Kim, H.J. Koo, et al., Oxygen-carrying micro/nanobubbles: composition, synthesis techniques and potential prospects in photo-triggered theranostics, Molecules 23 (2018).

[14] A. Sharma, J.F. Arambula, S. Koo, R. Kumar, H. Singh, J.L. Sessler, et al., Hypoxia-targeted drug delivery, Chem. Soc. Rev. 48 (2019) 771–813.

[15] W.R. Wilson, M.P. Hay, Targeting hypoxia in cancer therapy, Nat. Rev. Cancer 11 (2011) 393–410.

[16] M. Liu, A.R. Khan, J. Ji, G. Lin, X. Zhao, G. Zhai, Crosslinked self-assembled nanoparticles for chemo-sonodynamic combination therapy favoring antitumor, antimetastasis management and immune responses, J. Contr. Release 290 (2018) 150–164.

[17] Z. Chu, T. Tian, Z. Tao, J. Yang, B. Chen, H. Chen, et al., Upconversion nanoparticles@AgBiS2 core-shell nanoparticles with cancer-cell-specific cytotoxicity for combined photothermal and photodynamic therapy of cancers, Bioact. Mater. 17 (2022) 71–80.

[18] H.C. Yang, Q.Y. Wu, L.S. Wan, Z.K. Xu, Polydopamine gradients by oxygen diffusion controlled autoxidation, Chem. Commun. (Camb) 49 (2013) 10522–10524.

[19] C. Zhang, K. Pu, Molecular and nanoengineering approaches towards activatable cancer immunotherapy, Chem. Soc. Rev. 49 (2020) 4234–4253.

[20] R.P. Seekell, A.T. Lock, Y. Peng, A.R. Cole, D.A. Perry, J.N. Kheir, et al., Oxygen delivery using engineered microparticles, Proc. Natl. Acad. Sci. U. S. A. 113 (2016) 12380–12385.

[21] J.N. Kheir, L.A. Scharp, M.A. Borden, E.J. Swanson, A. Loxley, J.H. Reese, et al., Oxygen gas-filled microparticles provide intravenous oxygen delivery, Sci. Transl. Med. 4 (2012) 140ra88.

[22] M.S. Khan, J. Hwang, K. Lee, Y. Choi, J. Jang, Y. Kwon, et al., Surface composition and preparation method for oxygen nanobubbles for drug delivery and ultrasound imaging applications, Nanomaterials 9 (2019).

[23] A. Babaei, S. Moradi, Z. Hoseinkhani, D. Rezazadeh, S. Dokaneheifard, R. Asadpour, et al., Expression of hypoxia-inducible factor1-alpha in varicocele disease: a comprehensive systematic review, Reprod. Sci. (2021).

[24] A.T. Henze, M. Mazzone, The impact of hypoxia on tumor-associated macrophages, J. Clin. Invest. 126 (2016) 3672–3679.

[25] Q. Wu, W. Zhou, S. Yin, Y. Zhou, T. Chen, J. Qian, et al., Blocking triggering receptor expressed on myeloid cells-1-positive tumor-associated macrophages induced by hypoxia reverses immunosuppression and anti-programmed cell death ligand 1 resistance in liver cancer, Hepatology 70 (2019) 198–214.

[26] A. Watad, H. Rowe, T. Russell, Q. Zhou, L.K. Anderson, A. Khan, et al., Normal human enthesis harbours conventional CD4+ and CD8+ T cells with regulatory features and inducible IL-17A and TNF expression, Ann. Rheum. Dis. 79 (2020) 1044–1054.

[27] G. Petroni, A. Buque, L. Zitvogel, G. Kroemer, L. Galluzzi, Immunomodulation by targeted anticancer agents, Cancer Cell 39 (2021) 310–345.

[28] C.S. Yuan, Z.W. Deng, D. Qin, Y.Z. Mu, X.G. Chen, Y. Liu, Hypoxia-modulatory nanomaterials to relieve tumor hypoxic microenvironment and enhance immunotherapy: where do we stand? Acta Biomater. 125 (2021) 1–28.

[29] P. Prasad, C.R. Gordijo, A.Z. Abbasi, A. Maeda, A. Ip, A.M. Rauth, et al., Multifunctional albumin-MnO(2) nanoparticles modulate solid tumor microenvironment by attenuating hypoxia, acidosis, vascular endothelial growth factor and enhance radiation response, ACS Nano 8 (2014) 3202–3212.

[30] R.Q. Li, C. Zhang, B.R. Xie, W.Y. Yu, W.X. Qiu, H. Cheng, et al., A two-photon excited O2-evolving nanocomposite for efficient photodynamic therapy against hypoxic tumor, Biomaterials 194 (2019) 84–93.

[31] R. Zhang, X. Song, C. Liang, X. Yi, G. Song, Y. Chao, et al., Catalase-loaded cisplatin-prodrug-constructed liposomes to overcome tumor hypoxia for enhanced chemo-radiotherapy of cancer, Biomaterials 138 (2017) 13–21.

[32] M. Gao, C. Liang, X. Song, Q. Chen, Q. Jin, C. Wang, et al., Erythrocyte-membrane-enveloped perfluorocarbon as nanoscale Artificial red blood cells to relieve tumor hypoxia and enhance cancer radiotherapy, Adv. Mater. 29 (2017).

[33] C. Bialas, C. Moser, C.A. Sims, Artificial oxygen carriers and red blood cell substitutes: a historic overview and recent developments toward military and clinical relevance, J. Trauma Acute Care Surg. 87 (2019) S48–S58.

[34] J. Jagers, A. Wrobeln, K.B. Ferenz, Perfluorocarbon-based oxygen carriers: from physics to physiology, Pflügers Archiv 473 (2021) 139–150.

[35] S. Wilhelm, A.J. Tavares, Q. Dai, S. Ohta, J. Audet, H.F. Dvorak, et al., Analysis of nanoparticle delivery to tumours, Nat. Rev. Mater. 1 (2016), 16014.

[36] H.J. Mehta, A. Begnaud, A.M. Penley, J. Wynne, P. Malhotra, S. Fernandez-Bussy, et al., Treatment of isolated mediastinal and hilar recurrence of lung cancer with bronchoscopic endobronchial ultrasound guided intratumoral injection of chemotherapy with cisplatin, Lung Cancer 90 (2015) 542–547.

[37] X. Zheng, B.A. Goins, I.L. Cameron, C. Santoyo, A. Bao, V.C. Frohlich, et al., Ultrasound-guided intratumoral administration of collagenase-2 improved liposome drug accumulation in solid tumor xenografts, Cancer Chemother. Pharmacol. 67 (2011) 173–182.

[38] X. Song, J. Xu, C. Liang, Y. Chao, Q. Jin, C. Wang, et al., Self-supplied tumor oxygenation through separated liposomal delivery of H2O2 and Catalase for enhanced radio-immunotherapy of cancer, Nano Lett. 18 (2018) 6360–6368.

[39] A.J. Boutilier, S.F. Elsawa, Macrophage polarization states in the tumor microenvironment, Int. J. Mol. Sci. (2021) 22.

[40] L. Guo, H. Li, T. Fan, Y. Ma, L. Wang, Synergistic efficacy of curcumin and anti-programmed cell death-1 in hepatocellular carcinoma, Life Sci. 279 (2021), 119359.

[41] C. Yi, L. Chen, Z. Lin, L. Liu, W. Shao, R. Zhang, et al., Lenvatinib targets FGF receptor 4 to enhance antitumor immune response of anti-programmed cell death-1 in HCC, Hepatology 74 (2021) 2544–2560.

[42] Y. Lu, D. Xin, L. Guan, M. Xu, Y. Yang, Y. Chen, et al., Metformin downregulates PD-L1 expression in esophageal squamous cell catrcinoma by inhibiting IL-6 signaling pathway, Front. Oncol. 11 (2021), 762523.

[43] E. Chen, E. Li, H. Liu, Y. Zhou, L. Wen, J. Wang, et al., miR-26b enhances the sensitivity of hepatocellular carcinoma to Doxorubicin via USP9X-dependent degradation of p53 and regulation of autophagy, Int. J. Biol. Sci. 17 (2021) 781–795.